Repetitive High-Voltage Pulse Generator Based on Thermally Depolarized Ferroelectrics

Mihai Ganciu*, Oana Cramariuc

IT Center for Science and Technology, Bucharest, Romania

Andrei Petre Sebe

Sebit IT Consulting SRL, Bucharest, Romania

Răzvan Mircioaga

Military Technical Academy, Bucharest, Romania

Andrei Ludu†

Embry-Riddle Aeronautical University, Department of Mathematics & Wave Lab, Daytona Beach, FL 32114, USA

Abstract

We present a repetitive, non-destructive system for generating high-voltage pulses through fast, controlled thermal depolarization of pre-polarized ferroelectric ceramics. This system represents a significant advance in compact pulsed-power devices, where energy is stored in pre-polarized ferroelectrics. In our device, the ferroelectric pre-polarized ceramic is heated above the Curie temperature in a short, well-defined time interval, releasing the stored electrostatic energy bound by spontaneous polarization as a high-voltage pulse with rise times in the 20–50 ns range, peak amplitudes between 50 and 500 kV, and repetition rates from 0.1 to 10 Hz without material degradation. The system incorporates dedicated subsystems for rapid heating, liquid dielectric insulation, reverse-current blocking, adjustable spark-gap switching, nanosecond-scale diagnostics, and active cooling. Applications include high-power microwave generation, compact X-ray

flash radiography, high-power laser pumping, and various medical and industrial sectors requiring compact, reusable pulsed-power sources.

Corresponding authors:

* mihai.ganciu.phys@gmail.com
† ludua@erau.edu

1. Introduction

The generation of high-power electromagnetic pulses remains a critical challenge across multiple domains of modern technology, from inertial confinement fusion to directed energy applications and advanced diagnostic systems [1–8]. Traditional capacitor-based pulsed-power systems, while reliable, face fundamental limitations in energy density and portability that restrict their deployment in field applications and miniaturized systems [1–5]. Ferroelectric generators (FEGs) offer a compelling alternative by exploiting the rapid depolarization of pre-polarized ferroelectric ceramics to produce ultra-fast, high-voltage pulses in the 100–500 kV range with power outputs reaching gigawatt levels [1–8, 12, 13].

The operational principle of FEGs relies on mechanically induced phase transitions in ferroelectric materials. When a ferroelectric ceramic such as lead zirconate titanate (PZT) or lead lanthanum zirconate titanate (PLZT) is subjected to shock loading—typically generated by high-explosive detonation—the resulting stress wave drives a rapid transition from the polarized ferroelectric phase to a non-polar or differently oriented state [1–5]. This shock-induced depolarization releases bound charge at nanosecond timescales, generating electromagnetic pulses with rise times on the order of tens to hundreds of nanoseconds [11, 12, 14, 15]. The energy density achievable in these compact systems can exceed that of conventional capacitors by an order of magnitude, with values approaching 1–2 MJ/kg, making FEGs particularly attractive for applications where size, weight, and stored energy are critical constraints [8, 15, 16, 24].

The relevance of FEGs spans several high-impact technological domains. In fusion energy research, they provide intense electromagnetic fields necessary for magnetic flux compression and fast ignition schemes in inertial confinement fusion [12, 13]. Military applications exploit their ability to generate electromagnetic interference pulses and drive high-power microwave sources. In medical and industrial sectors, FEGs enable compact X-ray flash radiography systems and high-power laser pumping configurations [5–8, 12,

13]. Despite these diverse applications, significant challenges remain in optimizing the coupling between mechanical shock parameters and electrical output characteristics, understanding the complex material response under extreme loading conditions, and developing predictive models that can guide the design of next-generation ferroelectric pulse generators [12, 13].

Explosive FEGs [11, 14-16, 20, 21] rely on mechanically or detonation-induced depolarization to produce high-voltage pulses in the 100–500 kV range, but they are inherently single-shot, destructive devices that require handling of energetic materials and raise substantial operational safety and logistical issues. Classical work on completely explosive pulsed-power mini-systems and high-explosive pulsed power has identified attractive energy densities but also highlighted constraints related to reusability, test throughput, and integration in civilian laboratories [12, 13].

In parallel, the physics of thermally driven depolarization in ferroelectrics has been extensively studied, with detailed analyses of temperature-dependent spontaneous polarization, domain dynamics, and phase transitions at the Curie temperature T_c in materials such as $BaTiO_3$, PZT, and related solid solutions [11, 12, 14, 15]. Foundational references [11, 23, 24] describe the evolution from historical ferroelectric ceramics toward engineered compositions and domain structures, addressing applications in memories, actuators, and sensors rather than compact pulsed-power generators.

This paper presents a novel approach in the field of FEGs where, instead of obtaining fast depolarization of the ceramic sample using a shock wave, we demonstrate that the same result can be obtained through fast thermal depolarization above the Curie point of the ceramic. The system presented here eliminates the problem of device destruction after each pulse, in addition to providing the benefits of a safe working environment without the use of high explosives. Furthermore, by introducing a procedure of rapid forced cooling, we increase the repetition rate to 10 pulses per second.

The paper is organized as follows: in Section 2 we present the theoretical background and the physical processes of depolarization by shock waves and thermal wavefronts. Section 3 describes the system architecture. Section 4 describes the process of rapid heating and reverse-current blocking, while Section 5 describes the spark-gap switching systems. The full operating cycle is described in Section 6, and an example of experimental realization is introduced in Section 7. In Section 8 (Conclusions), we present a comparison with explosive FEGs, discuss various limitations, and provide examples of applications and other possible advanced architectures.

2. Theoretical Background on Thermal Depolarization

Ferroelectric materials exhibit a non-zero spontaneous polarization below T_c, associated with a symmetry-broken crystal structure and the presence of polar domains separated by domain walls [11, 12, 14]. As temperature approaches Tc from below, the magnitude of spontaneous polarization decreases rapidly, and at Tc the material undergoes a ferroelectric-to-paraelectric phase transition in which long-range polar order vanishes, releasing the energy stored in the ordered domain configuration.

The depolarization of ferroelectric material by a shock wave is a complex process involving several interrelated physical mechanisms at the molecular/atomic scale [1–8, 14-16]. On one hand, a shock wave creates an intense, rapid pressure pulse that mechanically distorts the crystal lattice, reorients dipole moments, and switches domains to energetically favorable orientations. Sufficiently strong shock compression also drives the material through phase transitions, causing the ferroelectric to lose polar symmetry above a critical pressure analogous to the Curie temperature effect. On the other hand, shock compression generates significant heating through plastic work and compression. This temperature rise reduces spontaneous polarization (approaching the Curie point) and increases thermal fluctuations that can randomize dipole orientations. The net result is typically a substantial loss of the macroscopic polarization that was present before the shock wave arrived, converting the stored electrostatic energy into charge flow (the depoling current) [17]. Consequently, detonation-induced depolarization not only destroys the entire system and prevents any repeatability of the experiment with the same sample, but the depolarization mechanism appears to be primarily mechanically stress-driven disruption, where thermal (Curie point) depolarization by phase transition is a secondary effect [14-16, 24].

In contrast, thermal depolarization at the Curie temperature is fundamentally a thermodynamic phase transition driven by the competition between ordering energy and thermal entropy. Below the Curie temperature Tc, in the ferroelectric phase, the free energy of the sample has multiple equivalent minima corresponding to different polarization directions, and thermal fluctuations cannot spontaneously depolarize the material. In Landau-Devonshire theory [13, 23, 24], the spontaneous polarization P minimizes the expression of the free energy $F(P,T) = F_0 + \propto_0 (T - Tc)^2 + \beta P^4 + \gamma P^6 + \cdots$ with temperature-dependent coefficients [11, 12, 23, 24]. When temperature exceeds the Curie point T_c, thermal energy disrupts the cooperative alignment interactions between dipoles, and the material undergoes a first-order phase transition to a non-polarized paraelectric phase. Unlike shock depolarization which fragments ferroelectric domains chaotically, thermal depolarization causes domains to simply cease to exist as meaningful entities, and the entire material uniformly transitions to the paraelectric state where there are no preferred polarization directions. The key distinction from shock depolarization is that the pure thermal process is an equilibrium

thermodynamic transition where the system smoothly evolves to minimize free energy, rather than a non-equilibrium mechanical disruption of an otherwise stable state.

However, by selecting compositions with Curie temperatures in the 300–420 K range and a narrow transition window of 10–30 K, such as $Ba_{0.87}Sr_{0.13}TiO_3$, $Ba_{0.88}Sr_{0.12}TiO_3$, $Ba_{0.90}Ca_{0.10}TiO_3$, $BaTi_{0.92}Sn_{0.08}O_3$ (BTS-8), or $Ba_{0.80}Pb_{0.20}TiO_3$ (BPT-20), the change in spontaneous polarization can be made abrupt and well localized in temperature [23, 24]. When such a body is pre-polarized and then heated rapidly through T_c under open-circuit or quasi-open-circuit conditions, the resulting depolarization manifests as a sharp rise in terminal voltage, which can be harvested as a high-voltage pulse [11, 12, 14, 23, 24].

3. System Architecture

The proposed FEG device consists mainly of a cylindrical polarized ferroelectric element with high-electrical-conductivity metal depositions (electrodes) on its lids, submerged in a liquid dielectric bath (see Fig. 1). In addition, we place a rapid heating system coaxial to the ferroelectric element and an active cooling assembly. In this way, a thermal pulse generated by the heating device depolarizes the ferroelectric sample, and the free electric charge is collected from the electrodes. As soon as the depoling current is collected into an electric load, and even while the sample is still warm above the Curie point, a continuous DC potential is immediately applied from an external source to the same probe electrodes, inducing a realignment field on the dipoles. Simultaneously, a fast-cooling system activates. This system consists of two symmetrically placed Peltier elements attached to the container (see Fig. 1) and two micro-turbine pumps that induce forced convection in the surrounding dielectric liquid. When the temperature drops below the Curie point, the sample is repolarized and ready for the next discharge. Additionally, the system contains a reverse-current blocking circuit, an adjustable spark-gap switch, and a high-bandwidth measurement and triggering subsystem.

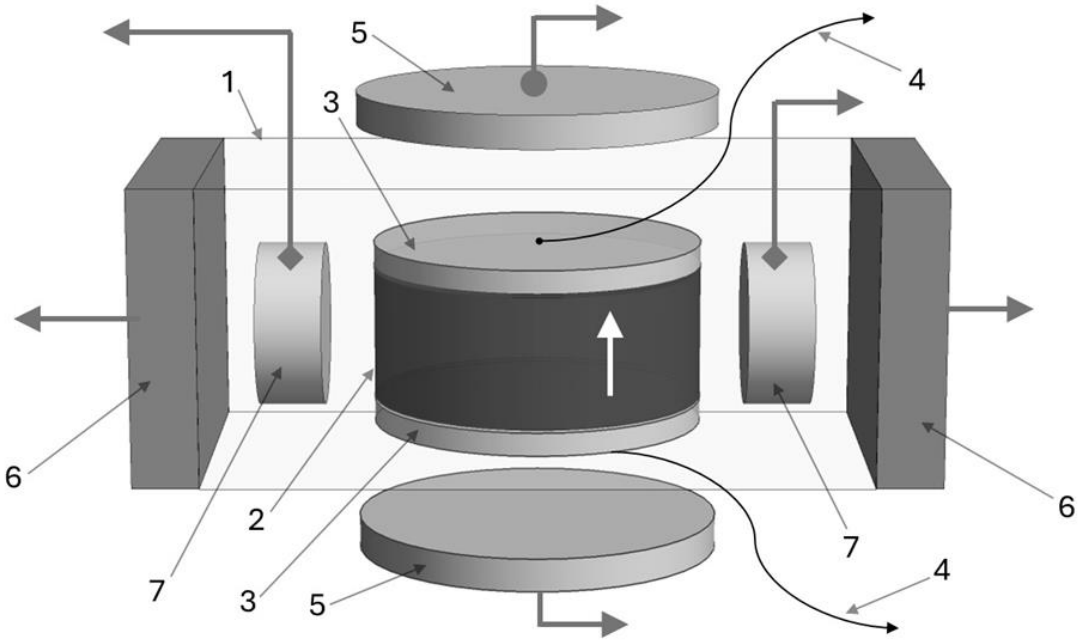

Fig. 1. The components of the pulse generator: In a silicone oil container (1) we place the pre-polarized ferroelectric sample with cylindrical geometry (2), where the axial polarization vector is indicated by the white arrow. The ferroelectric disk has surface depositions of high-electrical-conductivity metals (3) on its lids from which electrical terminals (4) are soldered. Two micro-turbine pumps (7) and two symmetrically placed cooling solid-state Peltier elements (6) ensure fast and uniform re-cooling of the sample (3). The ferroelectric is depolarized in a controlled thermal shock by two symmetrically placed lattices of IR lasers (LEDs, 5).

For experimental purposes, the ferroelectric element is typically a disk of $BaTiO_3$-based or PZT-type ceramic with a diameter of 20–40 mm and a thickness of 10–25 mm, metallized on opposite faces with Ag or Pt layers and bonded to copper electrodes for low-inductance connections. The body is pre-polarized at electric fields on the order of 3 kV/mm, either in a dedicated step at elevated temperature or by maintaining a DC bias during operation, ensuring a high initial level of remanent polarization around 40 $\mu C/cm^2$.

The ferroelectric element is immersed in a liquid dielectric such as silicone oil (e.g., Dow Corning 200, 10 cSt), which provides high dielectric strength, uniform heat transfer, and mechanical protection in a stainless-steel vessel with at least one transparent face for optical access. The oil volume, typically between 5 and 50 L, is managed through filtration and temperature control in the 15–60 °C range to guarantee stable electrical and thermal properties.

4. Rapid Heating and Reverse-Current Blocking

Fast thermal excitation is achieved using three alternative or combined approaches: resistive heating, optical heating, or hybrid heating. In the resistive option, a thin Ni-Cr foil of 50–100 μm thickness is attached to one electrode and driven by low-voltage, high-power DC sources (10–50 V, up to several hundred watts), enabling heating rates in the 0.5–10 K/ms range and, for optimized geometries, up to 10–100 K/ms. Optical heating employs xenon flash lamps, halogen lamps, or IR diode laser arrays, either coupled through the dielectric liquid or via optical fibers, providing flexible spatial and temporal control of the heat flux. A hybrid configuration combines IR and visible radiation to tailor the thermal front, improving uniformity and minimizing thermal gradients and mechanical stress in the ceramic body.

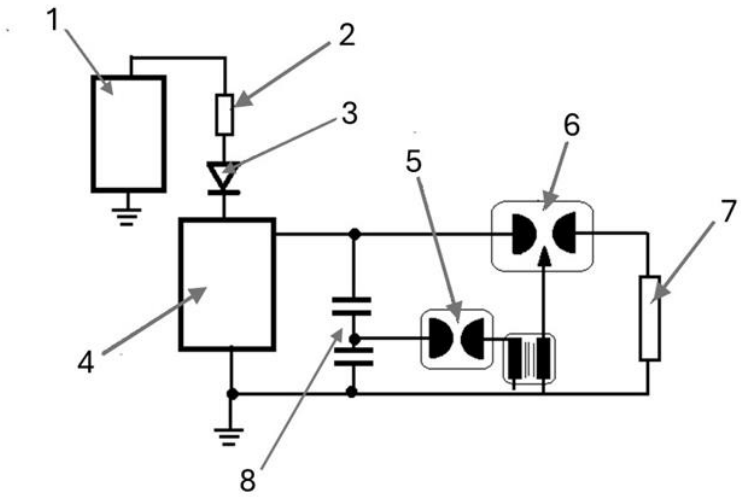

Fig. 2. The electrical diagram of the system. The ferroelectric sample (1) generates the high-voltage pulse through a limiting resistor (2) and a protective diode stack (3) into the ferroelectric thermal module (4). Spark-gap switches (5, 6) and capacitive dividers (8) ensure fast switching of the high-voltage pulse to the load (7).

The reverse-current blocking circuit is implemented as a stack of one to five high-voltage diodes connected in series with the ferroelectric element and the DC polarization source, dimensioned for up to 50 kV reverse bias and leakage currents on the order of tens of microamperes (Fig. 2). This stack prevents back-discharge into the polarization supply when the depolarization-induced voltage overshoots the DC level, while allowing normal charging currents during polarization and between pulses.

5. Spark-Gap Switching and Diagnostics

Energy transfer to the external load is controlled by a main spark-gap switch [20–22] with adjustable electrode spacing between 1 and 15 mm, using electrode materials such as tungsten, copper, or stainless alloys in gases like dry air or SF_6 at pressures from 0.5 to 5 atm (see Fig. 2). The device can operate in self-breakdown mode when the ferroelectric voltage exceeds the gas breakdown threshold or in trigger mode via an auxiliary spark-gap and a pulse transformer, using a high-voltage pulse generator such as in [22] or future optical triggering schemes [17, 18].

The diagnostic subsystem comprises at least two capacitive voltage dividers connected in parallel with the ferroelectric and/or the load: a slow, high-ratio divider for DC and low-frequency monitoring, and a fast, nanosecond-response divider for capturing the pulse waveform. Signals are recorded with digital oscilloscopes in the 200 MHz–1 GHz bandwidth and 1–10 GS/s sampling rate, while a programmable logic controller or equivalent coordinates threshold detection, trigger generation, and safety interlocks.

6. Operating Cycle

A typical operating cycle begins with preparation and polarization, where the ferroelectric element is brought to a temperature below Tc and polarized either in a separate pre-poling process or by connecting a DC high-voltage supply through the resistor-diode chain. In the subsequent heating phase, the resistive or optical heating subsystem is activated to drive the element temperature across Tc within a target time window of 60–300 ms, during which the terminal voltage rises from a baseline of around 40 kV to a maximum in the 50–500 kV range, depending on material and geometry. As the ferroelectric voltage approaches a predefined fraction of the expected peak (for example, 90%), the fast capacitive divider and comparator generate a trigger signal that initiates conduction in the main spark-gap, often via an auxiliary trigger circuit, thereby connecting the ferroelectric to the external load. The resulting high-voltage pulse exhibits rise times of 30–50 ns and full-width at half-maximum durations of 120–200 ns, delivering the stored energy to loads that may include resistive terminations, nonlinear transmission lines, or high-power microwave (HPM) structures. After each discharge, the cooling subsystem—combining natural convection in the oil, forced circulation at flows on the order of 10 L/min, and Peltier modules in advanced configurations—reduces the ferroelectric temperature back below Tc within tens of seconds, enabling repetition rates from 0.1 to several hertz depending on design. Material repolarization can be performed periodically to compensate for any gradual reduction in remanent polarization, although experimental results indicate stable operation over hundreds to a thousand cycles without significant degradation.

7. Experimental Realizations

In a first demonstrative configuration, a pre-polarized $BaTiO_3$-derived ceramic (e.g., BTS-8 or BPT-20) with a diameter of approximately 50 mm and thickness 5–15 mm is heated resistively by a 100 μm Ni-Cr foil in a 5 L silicone oil tank with two transparent windows. The system uses one or more series high-voltage diodes with microampere-level leakage currents, an adjustable air or nitrogen spark-gap, and a 50 Ω resistive load for monitoring, together with a GHz-class oscilloscope and capacitive divider.

For heating rates around 50 K/ms and repetition rates near 1 Hz, expected results include peak voltages of 50–85 kV on the load, rise times of 35 ± 8 ns, pulse energies consistent with 60–75% energy transfer efficiency, and stable performance over up to 1000 cycles without visible microcracking, delamination, or loss of bulk resistivity. Thermal measurements with K-type thermocouples at multiple radial positions and electrical measurements of amplitude, rise time, jitter, and repetition rate provide comprehensive characterization of the system dynamics.

A second configuration explores continuous polarization, where an initially un-poled $BaTiO_3$-based element is continuously biased at approximately 40 kV via a resistor and diode stack, while heating is provided by a 550 W IR LED or lamp. In this regime, reported or expected performance includes 70–80 kV peak output, rise times of 42 ± 7 ns, jitter of 80 ± 12 ns, and repetition rates from 0.5 to 10 Hz, with material integrity verified by SEM inspection and remanent polarization measurements after hundreds of cycles.

8. Conclusions

In this paper we introduce a new type of FEG based on a controlled thermal depolarization process. The major advance of such a system consists of its non-destructive, controllable, and repetitive generation of high-voltage pulses from ferroelectric ceramics. By combining fast thermal control, robust reverse-current protection, adjustable spark-gap switching, high-bandwidth diagnostics, and forced cooling, the system can deliver reusable high-voltage pulses suitable for integration into compact infrastructures. Its key advantage over known explosive FEG technologies lies in the non-explosive, safe, and repeatable nature, which opens new possibilities in industrial testing and scientific research (including medical fields) where high-performance electromagnetic sources must coexist with stringent safety and reusability requirements.

Compared to explosive ferroelectric pulsed-power systems, the present generator eliminates detonation and mechanical shock, relying instead on a purely thermal stimulus to trigger depolarization. This transition from explosive to controlled thermal depolarization removes the need for explosives handling, drastically improves operator and facility safety, and enables multi-shot, laboratory-friendly operation with programmable timing and repetition frequency.

Nevertheless, current implementations are limited to pulse amplitudes in the 50–500 kV range, below those achievable with large Marx generators or some high-explosive single-shot devices, and require non-negligible thermal management resources to sustain high repetition rates between 1 and 10 Hz. Mass, volume, and power-budget constraints must also be addressed for deployment on mobile platforms, where compactness, ruggedness, and autonomous operation are paramount.

Future developments of this project may include stacking multiple ferroelectric elements in series to increase output voltage, using parallel architectures to shape current and impedance, and exploring alternative geometries such as toroidal, ring-like, or segmented elements with multiple anodes to improve energy density and field uniformity. Hybrid depolarization schemes that combine thermal loading with mechanical compression or femtosecond-scale laser excitation are also envisioned to achieve sub-10-ns voltage rise times.

At the system level, the ferroelectric thermal depolarization generator may serve as a primary high-voltage source for an explosively pumped flux compression generator, followed by a vircator-based X-band stage and a polarization-controlled antenna. Target system parameters involve 100–500 kV input pulses with 10–50 ns rise time, 1–10 GW pulsed microwave output in the 8–12 GHz band, pulse durations of 10–100 ns, and jitter on the order of 10 ns, satisfying demanding requirements for research and defense electromagnetic applications. Practical applications range from electromagnetic jamming and temporary disruption of communications, navigation, and radar systems to durability testing of electronics under high-power electromagnetic pulse environments, high-power radar and ground-penetrating sensing, non-lethal neutralization of drones and autonomous vehicles, as well as plasma initiation and ultra-fast ionization and particle acceleration studies.

Acknowledgments

This work is related to OSIM patent application A/00573, November 24, 2024.

References

1. S. I. Shkuratov, J. Baird, V. G. Antipov, et al., Appl. Phys. Lett. **104**, 212901 (2014).

2. L. L. Altgilbers, M. D. J. Brown, I. Grishnaev, et al., *Magnetocumulative Generators* (Springer-Verlag, New York, 2000).

3. R. E. Setchell, J. Appl. Phys. **97**, 013507 (2005).

4. P. C. Lysne and C. M. Percival, J. Appl. Phys. **46**, 1519 (1975).

5. F. W. Neilson, Bull. Am. Phys. Soc. **2**, 302 (1957).

6. S. I. Shkuratov, J. Baird, E. F. Talantsev, et al., Sci. Rep. **2**, 931 (2012).

7. P. Shi, J. Liu, Y. Song, W. Wu, L. Liu, X. Zhou, X. Chen, X. Lou, and P. Liu, J. Appl. Phys. **135**, 124103 (2024) https://pubs.aip.org/aip/jap/article/135/12/124103/3278945

8. Y.-J. Gu, M. Jirka, O. Klimo, and S. Weber, Matter Radiat. Extremes **4**, 6 (2019) 064403 https://pubs.aip.org/aip/mre/article/4/6/064403/253056/Gamma-photons-and-electron-positron-pairs-from

9. L. Freeman, *Method for Derivation and Synthesis of Electromagnetic Environmental Effects Requirement Limits for Achieving System Level Electromagnetic Compatibility*, Electronic Theses and Dissertations (University of Central Florida 2016) https://stars.library.ucf.edu/etd/5215/

10. C. Wilson, *High altitude electromagnetic pulse (HEMP) and high power microwave (HPM) devices: Threat assessments*. No. CRSRL32544, Defense Tech. Inf. Center, Technical report ADA529982 (2008).

11. G. H. Haertling, J. Am. Ceram. Soc. **82**, 797 (1999).

12. M. E. Lines and A. M. Glass, *Principles and Applications of Ferroelectrics and Related Materials* (Oxford University Press, Oxford, 1977).

13. J. F. Scott, *Ferroelectric Memories* (Springer, Berlin, 2000).

14. D. Zhao et al., Nat. Commun. **10**, 3177 (2019).

15. V. Agrawal and K. Bhattacharya, Int. J. Solids Structures, **51**, 21-22 (2014) 3604-3618 https://www.sciencedirect.com/science/article/pii/S0020768314002534

16. E. F. Talantsev et al., Rev. Sci. Instruments **74**, 225 (2003).

17. E. W. Rosenthal et al., Opt. Express **28**, 24599 (2020).

18. J. Wang et al., IEEE Trans. Dielectr. Electr. Insul. **16**, 956 (2009).

19. U.S. Patent No. 4,845,378 A (1989)
https://patents.google.com/patent/US4845378A/en

20. S. I. Shkuratov, et al., *Completely explosive ultracompact high-voltage pulse generating system*, 2005 IEEE Pulsed Power Conference.

21. A. Ludu, P. Nicolau, and B. Novac, in *Megagauss Magnetic Field Generation and Related Topics*, edited by C. M. Fowler, R. Caird, and D. J. Erikson (Plenum Press, New York, 1986), pp. 369–375.

22. M. Ganciu et al., U.S. Patent No. 7,927,466 B2 (2007)
https://patents.google.com/patent/US7927466B2/zh

23. M. Acosta et al., Appl. Phys. Rev. **4**, 041305 (2017).

24. P. R. Potnis, N.-T. Tsou, and J. E. Huber, Materials **4**, 417 (2011).